

# Self-induced topological edge states in a lattice with onsite nonlinearity

Ruijiang Li<sup>1,\*</sup>, Wencai Wang<sup>1</sup>, Xiangyu Kong<sup>1</sup>, Ce Shang<sup>2</sup>,  
Yongtao Jia<sup>1</sup>, Gui-Geng Liu<sup>3,4,†</sup>, Ying Liu<sup>1</sup>, and Baile Zhang<sup>5,6‡</sup>

<sup>1</sup>*National Key Laboratory of Radar Detection and Sensing,*

*School of Electronic Engineering, Xidian University, Xi'an 710071, China*

<sup>2</sup>*Aerospace Information Research Institute, Chinese Academy of Sciences, Beijing 100094, China*

<sup>3</sup>*Research Center for Industries of the Future, Westlake University, Hangzhou, 310030, China*

<sup>4</sup>*Department of Electronic and Information Engineering,*

*School of Engineering, Westlake University, Hangzhou, 310030, China*

<sup>5</sup>*Division of Physics and Applied Physics, School of Physical and Mathematical Sciences,  
Nanyang Technological University, 21 Nanyang Link, Singapore 637371, Singapore and*

<sup>6</sup>*Centre for Disruptive Photonic Technologies, The Photonics Institute,  
Nanyang Technological University, 50 Nanyang Avenue, Singapore 639798, Singapore*

Topological edge states typically arise at the boundaries of topologically nontrivial structures or at interfaces between regions with differing topological invariants. When topological systems are extended into the nonlinear regime, linear topological edge states bifurcate into nonlinear counterparts, and topological gap solitons emerge in the bulk of the structures. Despite extensive studies of these two types of nonlinear states, self-induced topological edge states localized at the physical boundaries of originally nontopological structures remain underexplored. Unlike the previously reported self-induced topological transitions driven by nonlinear couplings, which are conceptually straightforward but less common in realistic interacting systems, here we experimentally realize self-induced topological edge states in a lattice with onsite nonlinearity. Leveraging the strong and tunable nonlinearity of electrical circuits, we systematically investigate the localized states in a nonlinear Su-Schrieffer-Heeger model. Besides revisiting the nonlinear topological edge states and topological gap solitons, we uncover a novel type of self-induced topological edge states which exhibit the hallmark features of linear topological edge states, including sublattice polarization, phase jumps, and decaying tails that approach zero. A distinctive feature of these states is the boundary-induced power threshold for existence. Our results are broadly applicable and can be readily extended to photonic and cold atomic systems, where onsite nonlinearities naturally arise from interparticle interactions. Our work unveils new opportunities for exploring novel correlated topological states of light and matter, and paves the way for the development of robust photonic devices and topological quantum computation.

Keywords: topological edge states; gap solitons; topological circuit; nonlinear lattice; Su-Schrieffer-Heeger model.

Topological insulators are physical structures that behave as conventional insulators in the bulk, but conducting on their surfaces due to the existence of topologically protected edge states [1, 2]. The realization of topological insulators has been demonstrated in diverse physical platforms, and the immunity of topological edge states to local deformations and disorders are of great significance for the exciting potential applications [3–12]. Extending topological insulators into the nonlinear regime such as by considering the nonlinear response of optical materials under high field intensity [13, 14], the interplay between topology and nonlinearity leads to the formation of the nonlinear topological edge states which bifurcate from the linear edge states and inherit topological protection from the linear counterparts [15–25]. In two-dimensional topological systems, due to the modulation instability, the nonlinear edge states develop into the edge solitons where dispersion is balanced with nonlinearity [15–17, 26–30]. The bifurcation from the linear topological states to the nonlinear ones is also applicable to the nonlinear higher-order topological systems, where nonlinear corner states are proposed [25, 31].

Topological gap solitons, which are self-localized topological states in the bulk with their spectra lie within the topological band gap, are also discovered in nonlinear topological systems [20, 22, 32–38]. Although the topological gap solitons have no direct linear counterparts, they exhibit the similar properties of the linear topological edge states, such as the sublattice polarization [22, 33, 35] and unidirectional transport [32, 37]. In contrast to the conventional lattice solitons which are self-localized due to the balance between coupling (commonly referred as diffraction in photonic systems) and nonlinearity, and thus are nontopological [39, 40], the topological gap solitons are localized at the nonlinearity-induced topological interfaces and their formation may be interpreted as the Jackiw-Rebbi Dirac boundary modes where mass inversion occurs across the interface [34, 35, 38].

Here, we investigate the topological states in the Su-Schrieffer-Heeger (SSH) model with onsite nonlinearity using electrical circuits [41]. Due to the flexibility of constructing the circuit lattices and the phase-resolved measurement technique, electrical circuits are particularly suited to probe the nonlinear topological physics

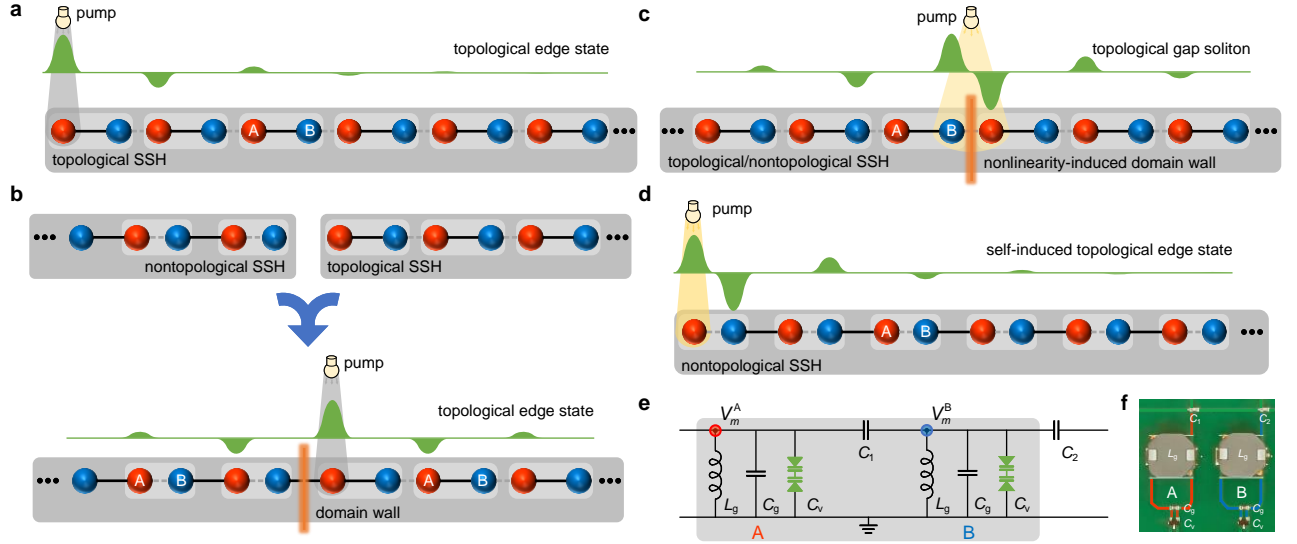


**FIG. 1. Schematics of the nonlinear SSH lattices and circuit realization.** **a**, A topological SSH lattice ending with weak bond. Under a weak pump, topological edge states appear at the left edge. **b**, A structure connected by two SSH lattices with different topological properties. Due to the formation of the domain wall, topological edge state also appears under a weak pump. With the increasing of pump intensity, the topological edge states in both **(a)** and **(b)** bifurcate to nonlinear ones. **c**, For a topological or nontopological SSH lattice, under the external pump, a nonlinearity-induced domain wall appears in the bulk and supports the formation of topological gap solitons. **d**, A nontopological SSH lattice ending with strong bond. Under the action of onsite nonlinearity, self-induced topological edge states appear at the physical termination. **e**, Circuit implementation of a unit cell in the lattices shown in **(a)**–**(d)**. The back-to-back varactor diodes provide the onsite nonlinearity of the SSH model. **f**, Unit cell of the experimentally realized circuit lattices.

[42–46]. As depicted in Fig. 1a, under a weak pump (i.e., in the linear limit), topological edge state appears at the edge of the topological SSH lattice (ending with strong bond). With the increasing of pump intensity, we observe the nonlinear topological edge states bifurcated from the linear counterpart. We experimentally validate the inherited properties of sublattice polarization and phase jump, and find that nonlinearity weakens the localization of the topological edge states. We then implement a structure by connecting two SSH lattices with different topological properties (Fig. 1b). Due to the formation of the domain wall, under a weak pump topological edge state appears as well. We experimentally reveal the similar state properties under increased pump intensity, because the nonlinear topological edge states in Figs. 1a–b have the same physical origin.

Different to the nonlinear topological edge states, topological gap solitons have no direct linear counterparts. For an SSH lattice (Fig. 1c), no matter the lattice is topological or nontopological in the linear limit, under the external pump, a nonlinearity-induced domain wall appears in the bulk and supports the formation of topological gap solitons. We experimentally observe that the left and right tails of the topological gap solitons have opposite sublattice polarizations, and reveal that nonlinearity increases the localization of the topological gap solitons. These features are in contrast to those of nonlinear topological edge states because the physical origins

are totally different.

Besides the nonlinear topological edge states and topological gap solitons, we discover both theoretically and experimentally an exotic type of topological states residing at the edge of a semi-infinite lattice ending with strong bond (Fig. 1d). Although the lattice is nontopological in the linear limit, under the action of onsite nonlinearity, it supports the self-induced topological edge states that reside at the physical termination of the structure. The self-induced edge states exhibit the sublattice polarization and phase jump starting from the second site close to the edge. They are the variant of the topological gap solitons under the breaking of the discrete translational symmetry at the structure edge, along with a boundary-induced power threshold for their existence. Specifically, the self-induced topological edge states can be approximately mapped to the linear topological edge state of a semi-infinite SSH lattice (Fig. 1a). Unlike the previously reported self-induced topological transitions driven by nonlinear couplings [42], which are conceptually straightforward but less common in realistic interacting systems, our self-induced topological edge states are realized in a lattice with onsite nonlinearity and feature decaying tails that approach zero, in contrast to the nonlocalized distributions that maintain non-zero plateau levels [42]. Our results are broadly applicable and can be readily extended to photonic and cold atomic systems, where

onsite nonlinearities naturally arise from interparticle interactions. Our work unveils new opportunities for exploring novel correlated topological states of light and matter, and paves the way for the development of robust photonic devices and topological quantum computation.

## Results

**Nonlinear SSH model realized using electrical circuits.** All the nonlinear SSH lattices shown in Figs. 1a-d can be realized using electrical circuits. Fig. 1e shows the circuit implementation of a unit cell, where A and B denote the two sublattice sites. For one sublattice, the inductor  $L_g$ , capacitor  $C_g$ , and back-to-back varactor diode  $C_v$  are wired in parallel. The varactor diode acts as a voltage-dependent variable capacitor with  $C_v = C_L + C_{NL}$ , where the linear part  $C_L$  is the capacitance at the zero voltage and the nonlinear part can be phenomenologically written as  $C_{NL} = -C_L + \frac{C_L}{(1+|v/v_0|)^M}$  (see Supplementary Note 1). Here,  $v_0$  and  $M$  are constants, and  $v$  is the voltage amplitude. The sublattice sites are wired with each other through the intracell coupling capacitor  $C_1$  and intercell coupling capacitor  $C_2$ .

For a typical SSH circuit that emulates the lattice shown in Fig. 1a, it can be described by the discretized Gross-Pitaevskii equation:

$$i \frac{d}{dt} \begin{bmatrix} V_m^A \\ V_m^B \end{bmatrix} = E_0 \begin{bmatrix} V_m^A \\ V_m^B \end{bmatrix} + J_1 \begin{bmatrix} V_m^B \\ V_m^A \end{bmatrix} + J_2 \begin{bmatrix} V_{m-1}^B \\ V_{m+1}^A \end{bmatrix} + \begin{bmatrix} g(V_m^A) V_m^A \\ g(V_m^B) V_m^B \end{bmatrix}, \quad (1)$$

where  $[V_m^A(t), V_m^B(t)]^T$  are the time-dependent voltages on sites A and B in the  $m$ th unit cell,  $E_0 = \omega_0 + \Delta E$  is equivalent to the constant onsite energy, which includes the resonant frequency of the linear oscillators  $\omega_0 = 1/\sqrt{L_g(C_g + C_L)}$  and the frequency shift induced by the coupling capacitors  $\Delta E = -\frac{C_1 + C_2}{2(C_g + C_L)}\omega_0$ ,  $J_1 = \frac{C_1}{2(C_g + C_L)}\omega_0$  and  $J_2 = \frac{C_2}{2(C_g + C_L)}\omega_0$  are the intracell and intercell coupling coefficients, respectively, and  $g(V_m^\sigma) = -\frac{C_{NL}(V_m^\sigma)}{2(C_g + C_L)}\omega_0$  ( $\sigma = A, B$ ) is the voltage-dependent onsite energy. Eq. (1) is valid under  $C_{1,2} \ll C_g + C_L$  and  $C_{NL} \ll C_g + C_L$ , where the slowly-varying envelope approximation holds (see Supplementary Note 2 for the derivation from the Kirchhoff circuit equations). Thus, the nonlinear circuit lattice realizes the SSH model with onsite nonlinearity, and the four lattice configurations shown in Figs. 1a-d all can be implemented based on the circuit dimer in Fig. 1e. Fig. 1f shows the unit cell of the experimentally realized circuit lattices.

**Nonlinear topological edge states.** We first study the nonlinear topological states in the SSH lattices shown in Fig. 1a. The configuration is a typical semi-infinite SSH lattice that ends with a weak bond. In the lin-

ear limit, due to the nontrivial topology with the winding number  $\mathcal{W} = 1$ , topological edge state residing at the left edge exists [41]. Under the action of the onsite nonlinearity, by bifurcating from the linear edge state, nonlinear topological edge states with the topological protection inherited from the linear counterpart appear (see Methods for the algorithm and Supplementary Note 3 for the stability analysis). As depicted in Fig. 2a, with the power increasing (defined as the sum of the squares of all the site voltages), the frequency of the nonlinear edge state exhibits a blue shift due to the decreased grounding capacitance, and the state localization becomes weak with a larger participation ratio defined as  $(\sum_{m,\sigma} |v_m^\sigma|^2)^2 / \sum_{m,\sigma} |v_m^\sigma|^4$  ( $\sigma = A, B$ ), particularly

when the frequency enters the linear bulk band (denoted by the shaded gray areas). The inset of Fig. 2a shows a typical profile of the nonlinear edge states. Since the nonlinear edge states are bifurcated from the linear counterpart which satisfies  $v_m^A = \left(-\frac{J_1}{J_2}\right)^{|m|} v_0^A$  and  $v_m^B = 0$ , their voltages mainly distribute on sublattice site A with the sublattice pseudospin

$$S = \frac{\sum_m |v_m^A|^2 - |v_m^B|^2}{\sum_m |v_m^A|^2 + |v_m^B|^2} \quad (2)$$

nearly equal to 1 and the phase jump of  $\pi$  among the neighboring cells.

Experimentally, we excite site 1 of the circuit lattice using an external input voltage with frequency sweep to observe the nonlinear topological edge states (see Methods and Supplementary Note 4 for the experimental implementation). From the experimental and theoretical results shown in Fig. 2b, under a small input voltage, the voltage spectrum exhibits a nearly symmetric peak with respect to the resonant frequency, indicating the presence of the topological edge state in the linear limit. As the input voltage increases, the spectrum peak becomes asymmetric and the resonant frequency exhibits a blue shift (see Supplementary Note 4 for the complete voltage spectra). We further extract the resonant frequencies under different input voltages and measure the voltage distributions in the circuit lattice. The normalized amplitudes and phases of the experimental voltage distributions are shown in Fig. 2c. At higher input voltages, the localization of the nonlinear edge state decreases, although the characteristics of sublattice polarization and phase jump remain intact (see Supplementary Note 4 for the quantitative analysis). This observation aligns with the theoretical prediction and confirms that nonlinearity weakens the localization of the nonlinear topological edge states.

We then study the second configuration shown in Fig. 1b. The structure is connected by two lattices with different topological properties defined in the linear limit

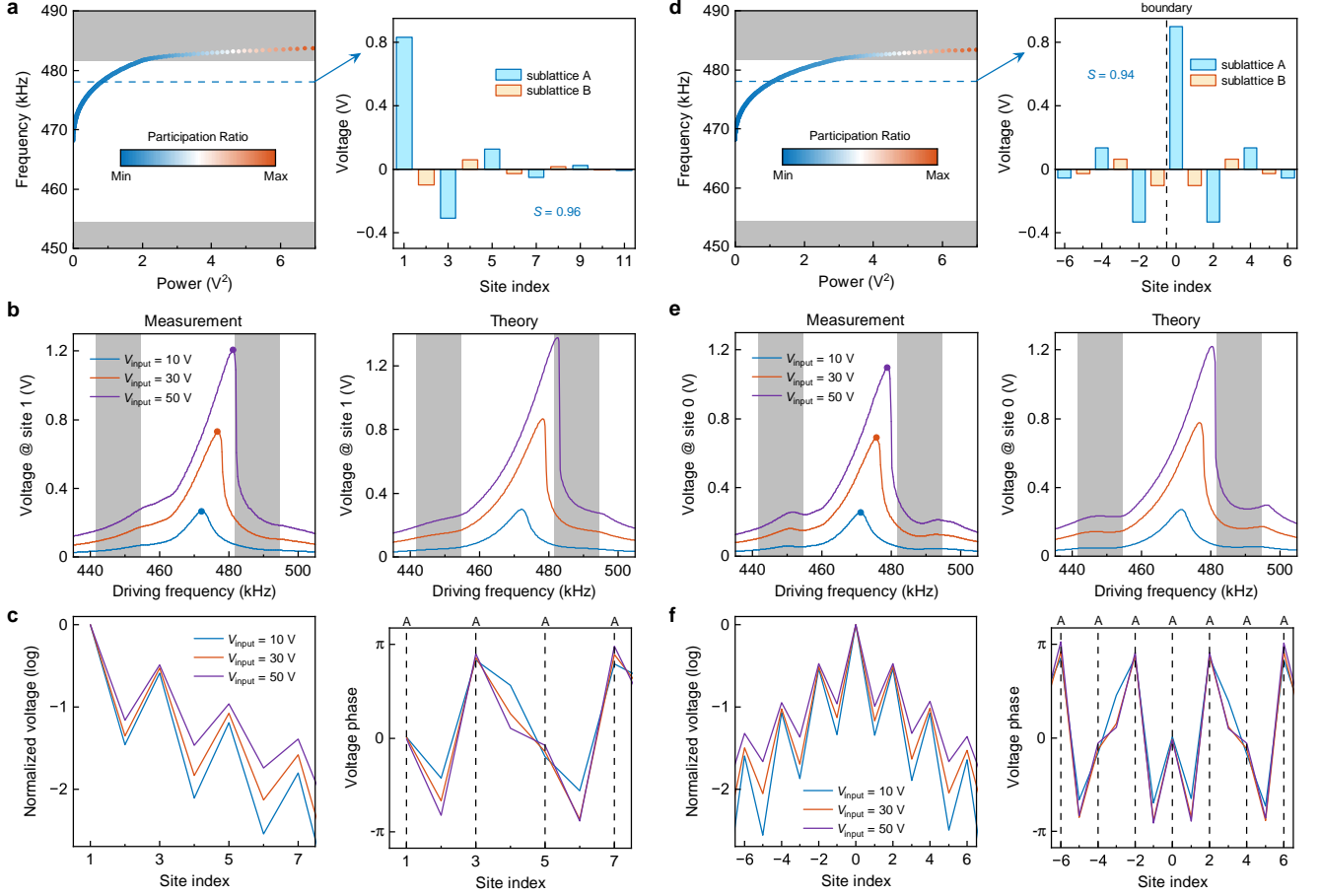


FIG. 2. **Nonlinear topological edge states.** **a**, Nonlinear topological edge states residing at the edge of a semi-infinite SSH lattice that ends with a weak bond. Participation ratio measures the state localization. The inset shows a typical voltage distribution of the nonlinear topological edge states. **b**, At different input voltages, the voltage spectra measured experimentally and calculated theoretically. **c**, The normalized amplitudes (left) and phases (right) of the experimental voltage distributions at the resonant frequencies indicated by the dots in (b). **d-f**, Results for the nonlinear topological edge states in a structure formed by connecting two lattices with different topological properties in the linear limit.

(winding number  $\mathcal{W} = 0$  for the left nontopological part and  $\mathcal{W} = 1$  for the right topological part [47]). Without nonlinearity, a topological edge state is localized at the boundary between the two parts [48, 49]. Similarly, with onsite nonlinearity, nonlinear topological edge states which are bifurcated from the linear edge state appear, as shown in Fig. 2d (see Supplementary Note 5 for the stability analysis). Due to the same physical origin, the nonlinear topological edge states in this lattice also exhibit the sublattice polarization and phase jump, and nonlinearity also weakens the state localization. These properties are confirmed by the experimental measurements presented in Figs. 2e-f (see Supplementary Note 6 for the experimental implementation, complete voltage spectra, and quantitative analysis). Note that the nonlinear topological edge states are completely different from the nontopological conventional solitons that do not possess these characteristics (see Supplementary Notes 5 for the nontopological edge states).

**Topological gap solitons.** We will now discuss the topological gap solitons in the lattice depicted in Fig. 1b. In contrast to the nonlinear topological edge states, the topological gap solitons lack a direct linear counterpart, although they reside spectrally within the SSH gap. From Fig. 3a, the topological gap solitons bifurcate from the edge of the linear Bloch band and converge to the bulk state in the linear limit (see Supplementary Note 7 for the bifurcation and stability). Under the influence of onsite nonlinearity, a topological interface can be induced at the center unit cell of the lattice [34, 35]. The Dirac mass defined as  $m_{\text{Dirac}} = \frac{g(V_m^A) - g(V_m^B)}{2}$  exhibits an inversion ( $m_{\text{Dirac}} > 0$  for the left part and  $m_{\text{Dirac}} < 0$  for the right part), and the topological gap solitons emerge as the Jackiw-Rebbi-type Dirac boundary modes (see Supplementary Note 7 for the physical interpretation). The nonlinearity-induced interface can also be interpreted as an impurity potential that splits the original lattice

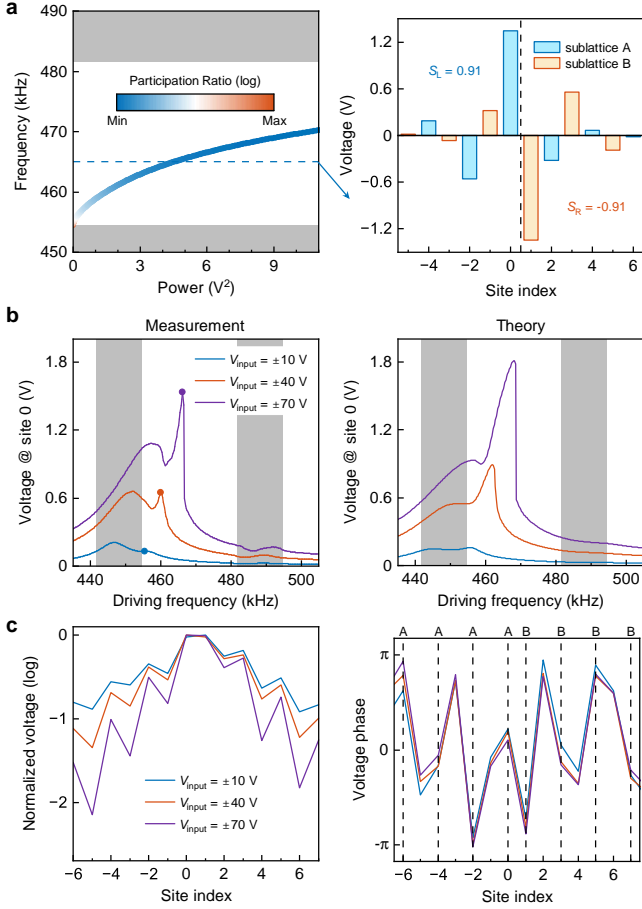


FIG. 3. **Topological gap solitons.** **a**, Frequencies and participation ratios of the topological gap solitons. The inset shows a typical voltage distribution of the topological gap solitons. **b**, Voltage spectra measured experimentally and calculated theoretically. **c**, The normalized amplitudes (left) and phases (right) of the experimental voltage distributions at the resonant frequencies indicated by the dots in (b).

into two topological regions, and the topological gap soliton represents a combination of the two topological edge states [20].

The global sublattice polarizations of the topological gap solitons vanish because the left and right tails exhibit opposite chiralities [22]. From the inset in Fig. 3a, the left tail is primarily confined to the sublattice site A, exhibiting a positive local sublattice pseudospin  $S_L$ , while the right tail displays a negative  $S_R$ . Experimentally, the topological gap solitons are excited using two out-of-phase input voltages, revealing the properties of both sublattice polarization and phase jumping, as shown in Figs. 3b-c (see Supplementary Note 8 for the comprehensive analysis and excitation of nontopological gap solitons). The small deviations in the voltage distributions from the perfectly symmetric profiles may result from imperfections in the circuit lattice and input voltages, as well as the limited temporal resolution in

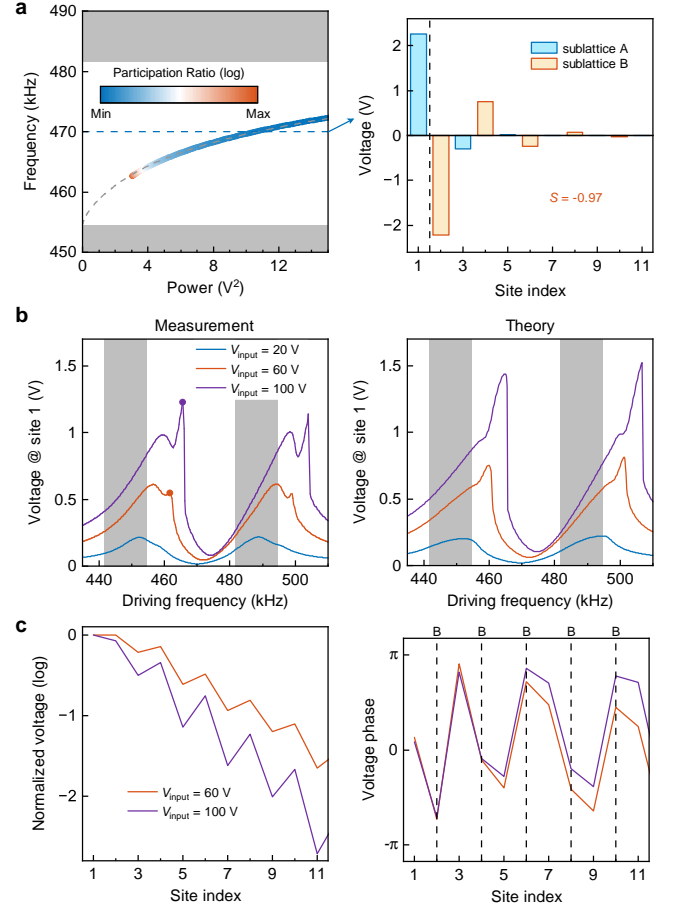


FIG. 4. **Self-induced topological edge states.** **a**, Frequencies and participation ratios of the self-induced topological edge states. For comparison, the frequencies of the topological gap solitons are also plotted. The inset shows a typical voltage distribution of the self-induced topological edge states. **b**, Voltage spectra measured experimentally and calculated theoretically. **c**, The normalized amplitudes (left) and phases (right) of the experimental voltage distributions at the resonant frequencies indicated by the dots in (b).

measurements (see Methods). Furthermore, since the topological gap solitons are nonlinearity-induced states, their localization is enhanced under stronger input voltages, provided that the delocalized gap solitons within the linear bulk band are not excited (see Supplementary Note 7).

**Self-induced topological edge states.** The nonlinear topological states we currently implement rely on a topological edge, whether it is the physical termination of a lattice or a topological interface induced by nonlinearity. Hereafter, we turn to a semi-infinite lattice ending with a strong bond (Fig. 1c), and show the emergence of an exotic type of nonlinear topological states that reside at the edge of a nonlinear nontopological lattice.

Fig. 4a shows the frequencies and participation ra-

tios of the self-induced topological edge states. Although topological edge states do not exist in the linear limit, above a certain power threshold, localized states with their maxima reside at the leftmost unit cell (see the inset of Fig. 4a) appear in the SSH gap. Neglecting the voltage at the first site, the self-induced edge state exhibits the similar profile with the nonlinear topological edge state (the inset of Fig. 2a) and half of the topological gap soliton (the inset of Fig. 3a). Considering the similarity, the self-induced topological edge states at the left edge can be created by the discrete translational transformation  $\mathcal{T}V_m^{A,B} = V_{m-1}^{A,B}$ , where  $\mathcal{T}$  is the translational operator. The power threshold is induced by the breaking of discrete translational symmetry when moving the topological gap solitons towards the edge (see Supplementary Note 9 for the relation between self-induced topological edge states and topological gap solitons). Since the circuit nonlinearity adds perturbations to the onsite energy, the self-induced topological edge states can be approximated using the solutions of Eq. (1) with  $g \neq 0$  for the leftmost unit cell and  $g = 0$  for the other sites. When the state frequency equals to the constant onsite energy  $E_0$ , i.e., the frequency of the linear topological edge state, the Gross-Pitaevskii equation reduces to

$$J_1 v_1^B + g(v_1^A) v_1^A = 0, \quad (3)$$

$$J_1 v_1^A + g(v_1^B) v_1^B = 0, \quad (4)$$

with  $v_m^B = \left(-\frac{J_1}{J_2}\right)^{|m|-1} v_1^B$  and  $v_m^A = 0$  for  $m \geq 2$  (see Supplementary Note 9). Eqs. (3)-(4) govern the voltage distributions in a single dimer and allow for an antisymmetric solution:  $v_1^A = -v_1^B$  with  $g(v_1^A) = J_1$ , which is consistent with the profile shown in the inset of Fig. 4a. The relationship between the voltages at the other sites is precisely analogous to that of a linear topological edge state. Thus, the self-induced topological edge states at a nontopological edge represent a continuation of the antisymmetric state in the anti-continuum limit (see Supplementary Note 9), and they can be approximately mapped to the linear topological edge state of a semi-infinite SSH lattice.

To experimentally probe the self-induced topological edge states, we excite the leftmost site, specifically site 1 of the circuit lattice. From Fig. 4b, no peak is observed in the SSH gap for  $V_{\text{input}} = 20$  V, indicating the presence of a power threshold for the self-induced topological edge states. The threshold value obtained from the excitation spectra deviates from the result in Fig. 4a possibly due to the excitation of other nonlinear states (see Supplementary Note 10). At high input voltages, the voltage distributions in Fig. 4c reveal that the self-induced topological edge states exhibit sublattice polarization and phase jump starting from the second site near the physical termination. Meanwhile, similar to the topological gap solitons, nonlinearity can

enhance the localization of self-induced topological edge states, unless the resonant frequency is driven into the linear bulk band, which is consistent with the theoretical prediction in Fig. 4a. Note that the resonant peak in the semi-infinite gap in Fig. 4b corresponds to the excitation of nontopological conventional solitons (see Supplementary Note 10 for the discussion on nontopological edge solitons).

**Conclusion.** This work experimentally and theoretically reveals the existence of the nonlinear topological edge states and topological gap solitons in SSH circuit lattices. Contrary to the conventional understanding of the bulk-boundary correspondence, we demonstrate the formation of the self-induced topological edge states that reside at the physical termination (rather than the nonlinearity-induced interface) of a nonlinear nontopological lattice. This exotic type of nonlinear topological states may pave the way to exploring intriguing topological states in more complex nonlinear topological systems, such as high-dimensional or higher-order systems, and the platform of nonlinear electrical circuits may be used to explore the interacting topological physics [50] (see Supplementary Note 2).

## Methods

**Sample fabrication and measurement.** The circuit parameters in the four SSH circuits are  $C_g = 4.7$  nF,  $L_g = 15$   $\mu$ H,  $C_L = 73.48$  pF,  $v_0 = 2.1935$ , and  $M = 0.4548$ . For the lattice shown in Fig. 1a, the intracell and intercell coupling capacitors are  $C_1 = 180$  pF and  $C_2 = 560$  pF, respectively. For the lattice shown in Fig. 1b, the topological part has  $C_1 = 180$  pF and  $C_2 = 560$  pF, while the nontopological part has  $C_1 = 560$  pF and  $C_2 = 180$  pF. An additional capacitance  $C_2 - C_1$  is added to the grounding capacitance of the interface circuit node. For the lattices shown in Fig. 1c-d, the intracell and intercell coupling capacitors are  $C_1 = 560$  pF and  $C_2 = 180$  pF, respectively.

To ensure the observation of nonlinear topological states, the circuit components should have minimal parasitic parameters, and their tolerance should be as low as possible. For this purpose, we utilize capacitors with low ESL and  $\pm 1\%$  tolerance. We also employ inductors with magnetic shielding and low DCR, and delicately select the components using an LCR meter (HIOKI IM3536). The tolerances for inductance and series resistance are  $\pm 1\%$  and  $\pm 2\%$ , respectively. The average series resistance of the inductors is approximately 600 m $\Omega$ ; however, it increases with higher frequencies and larger currents. To characterize the voltage response of varactor diodes (BB201), we measure the  $C$ - $V$  curves and the parameters  $C_L$ ,  $v_0$ , and  $M$  are obtained by fitting these curves with the phenomenological formula. We use standard PCB techniques to fabricate the lattice, ensuring that the inductors are sufficiently spaced to prevent mutual cou-

pling. The PCB traces have a relatively large width of 0.75 mm to accommodate high currents, and the layouts are carefully optimized to minimize parasitic parameters and coupling with other circuit components.

To excite the circuit lattices, SMA connectors are soldered onto PCB for signal injection from an arbitrary function generator (Tektronix AFG31022). Since the output voltage of an arbitrary function generator is typically low, we utilize a high voltage amplifier (Aigtek ATA-2022B) to amplify the voltage signals. However, due to bandwidth limitations, the output voltage of the high voltage amplifier may be lower than the preset value at high operating frequencies. Additionally, the output voltages of the independent channels may contain errors. To detect the voltage signals at the circuit nodes, home-made connectors on the PCB are connected to an oscilloscope (Tektronix MDO34). For the excitation spectrum measurement, we fix the input voltage and conduct program-controlled frequency sweeps, during which the voltage signals at the circuit nodes are recorded.

**Theoretical calculations.** To calculate the frequencies and voltage distributions of the nonlinear topological states, we solve the Gross-Pitaevskii equation [i.e., Eq. (1)] using the ansatz  $V_m^{A,B} = v_m^{A,B} \exp(-i\omega t)$ . We employ Newton's method to solve the eigenvalue equation for each  $\omega$ . Open boundary conditions are used to truncate the nonlinear circuit lattice. For the calculation of the nonlinear topological edge states, the linear topological edge states with scaling factors are taken as initial guesses. To calculate the topological gap solitons, self-induced topological edge states, and other nontopological solitons, we employ the anti-continuum approach. Once we obtain the soliton solution at a given  $\omega$ , solutions at other frequencies can be obtained iteratively. The stability of the nonlinear topological states is analyzed using the standard linear stability technique and subsequently confirmed through temporal evolution based on the Runge-Kutta algorithm.

The excitation spectra are calculated by solving the driven-dissipative Gross-Pitaevskii equation. Dissipation is characterized by  $\gamma$  at the input node and  $\gamma_L$  at the other nodes. Newton's method is employed to find the complex solutions. We calculate the voltage distributions at two frequencies away from the resonant frequencies, and use these solutions as initial guesses to obtain the entire spectrum. Finally, for a fixed driving voltage, we obtain two voltage spectra: one curve is obtained by increasing the driving frequency, while the other corresponds to a frequency sweep in the opposite direction. The bistable response can be observed by comparing the two voltage spectra.

## Acknowledgements

R.L., W.W. and X.K. was sponsored by the National Key Research and Development Program of China (Grant No. 2022YFA1404902) and National Natural

Science Foundation of China (Grant No. 12104353). Y.L. was sponsored by the National Natural Science Foundation of China (NSFC) under Grant No. 61871309 and the 111 Project. B.Z. acknowledges support from Singapore National Research Foundation Competitive Research Program Grant No. NRF-CRP23-2019-0007, Singapore Ministry of Education Academic Research Fund Tier 2 Grant No. MOE-T2EP50123-0007, and Tier 1 Grant No. RG81/23.

## Author contributions

R.L. conceived the idea and performed the theoretical calculations. R.L. and W.W. designed and conducted the experiments with the help of X.K. and Y.J. R.L., X.K., C.S., G.-G.L. and B.Z. wrote the manuscript. R.L., Y.L. and B.Z. supervised the project.

## Competing interest

The authors declare no competing financial interest.

## Data availability

The data that support the findings of this study are available from the corresponding authors upon reasonable request.

---

\* Corresponding author: rujiangli@xidian.edu.cn

† Corresponding author: liuguigeng@westlake.edu.cn

‡ Corresponding author: blzhang@ntu.edu.sg

- [1] Hasan, M. Z. & Kane, C. L. Colloquium: Topological insulators. *Rev. Mod. Phys.* 82, 3045-3067 (2010).
- [2] Qi, X.-L. & Zhang, S.-C. Topological insulators and superconductors. *Rev. Mod. Phys.* 83, 1057-1110 (2011).
- [3] Breunig, O. & Ando, Y. Opportunities in topological insulator devices. *Nat. Rev. Phys.* 4, 184-193 (2022).
- [4] Ma, G., Xiao, M. & Chan, C. T. Topological phases in acoustic and mechanical systems. *Nat. Rev. Phys.* 1, 281-294 (2019).
- [5] Xue, H., Yang, Y. & Zhang, B. Topological acoustics. *Nat. Rev. Mater.* 7, 974-990 (2022).
- [6] Cooper, N. R., Dalibard, J. & Spielman, I. B. Topological bands for ultracold atoms. *Rev. Mod. Phys.* 91, 015005 (2019).
- [7] Lin, Z.-K. et al. Topological phenomena at defects in acoustic, photonic and solid-state lattices. *Nat. Rev. Phys.* 5, 483-495 (2023).
- [8] Xie, B. et al. Higher-order band topology. *Nat. Rev. Phys.* 3, 520-532 (2021).
- [9] Shah, T., Brendel, C., Peano, V. & Marquardt, F. Colloquium: Topologically protected transport in engineered mechanical systems. *Rev. Mod. Phys.* 96, 021002 (2024).
- [10] Lu, L., Joannopoulos, J. D. & Soljačić, M. Topological photonics. *Nature Photon.* 8, 821-829 (2014).
- [11] Khanikaev, A. B. & Shvets, G. Two-dimensional topological photonics. *Nature Photon.* 11, 763-773 (2017).
- [12] Ozawa, T. et al. Topological Photonics. *Rev. Mod. Phys.* 91, 015006 (2019).
- [13] Smirnova, D., Leykam, D., Chong, Y. & Kivshar, Y. Non-



- linear topological photonics. *Appl. Phys. Rev.* 7, 021306 (2020).
- [14] Szameit, A. & Rechtsman, M. C. Discrete nonlinear topological photonics. *Nat. Phys.* 20, 905-912 (2024).
  - [15] Ablowitz, M. J., Curtis, C. W. & Ma, Y.-P. Linear and nonlinear traveling edge waves in optical honeycomb lattices. *Phys. Rev. A* 90, 023813 (2014).
  - [16] Lumer, Y., Rechtsman, M. C., Plotnik, Y. & Segev, M. Instability of bosonic topological edge states in the presence of interactions. *Phys. Rev. A* 94, 021801 (2016).
  - [17] Kartashov, Y. V. & Skryabin, D. V. Modulational instability and solitary waves in polariton topological insulators. *Optica* 3, 1228 (2016).
  - [18] Kartashov, Y. V. & Skryabin, D. V. Bistable Topological Insulator with Exciton-Polaritons. *Phys. Rev. Lett.* 119, 253904 (2017).
  - [19] Dobrykh, D. A., Yulin, A. V., Slobozhanyuk, A. P., Poddubny, A. N. & Kivshar, Yu. S. Nonlinear Control of Electromagnetic Topological Edge States. *Phys. Rev. Lett.* 121, 163901 (2018).
  - [20] Tuloup, T. Nonlinearity induced topological physics in momentum space and real space. *Phys. Rev. B* 102, 115411 (2020).
  - [21] Guo, M. et al. Weakly nonlinear topological gap solitons in Su-Schrieffer-Heeger photonic lattices. *Opt. Lett.* 45, 6466 (2020).
  - [22] Pernet, N. et al. Gap solitons in a one-dimensional driven-dissipative topological lattice. *Nat. Phys.* 18, 678-684 (2022).
  - [23] Kartashov, Y. V. et al. Observation of Edge Solitons in Topological Trimer Arrays. *Phys. Rev. Lett.* 128, 093901 (2022).
  - [24] Ma, Y.-P. & Susanto, H. Topological edge solitons and their stability in a nonlinear Su-Schrieffer-Heeger model. *Phys. Rev. E* 104, 054206 (2021).
  - [25] Ezawa, M. Nonlinearity-induced transition in the nonlinear Su-Schrieffer-Heeger model and a nonlinear higher-order topological system. *Phys. Rev. B* 104, 235420 (2021).
  - [26] Leykam, D. & Chong, Y. D. Edge Solitons in Nonlinear-Photonic Topological Insulators. *Phys. Rev. Lett.* 117, 143901 (2016).
  - [27] Ivanov, S. K., Kartashov, Y. V., Szameit, A., Torner, L. & Konotop, V. V. Vector Topological Edge Solitons in Floquet Insulators. *ACS Photonics* 7, 735-745 (2020).
  - [28] Zhang, Z. et al. Observation of edge solitons in photonic graphene. *Nat. Commun.* 11, 1902 (2020).
  - [29] Mukherjee, S. & Rechtsman, M. C. Observation of Unidirectional Solitonlike Edge States in Nonlinear Floquet Topological Insulators. *Phys. Rev. X* 11, 041057 (2021).
  - [30] Ezawa, M. Nonlinearity-induced chiral solitonlike edge states in Chern systems. *Phys. Rev. B* 106, 195423 (2022).
  - [31] Kirsch, M. S. et al. Nonlinear second-order photonic topological insulators. *Nat. Phys.* 17, 995-1000 (2021).
  - [32] Lumer, Y., Plotnik, Y., Rechtsman, M. C. & Segev, M. Self-Localized States in Photonic Topological Insulators. *Phys. Rev. Lett.* 111, 243905 (2013).
  - [33] Solnyshkov, D. D., Bleu, O., Teklu, B. & Malpuech, G. Chirality of Topological Gap Solitons in Bosonic Dimer Chains. *Phys. Rev. Lett.* 118, 023901 (2017).
  - [34] Poddubny, A. N. & Smirnova, D. A. Ring Dirac solitons in nonlinear topological systems. *Phys. Rev. A* 98, 013827 (2018).
  - [35] Smirnova, D. A., Smirnov, L. A., Leykam, D. & Kivshar, Y. S. Topological Edge States and Gap Solitons in the Nonlinear Dirac Model. *Laser & Photonics Rev.* 13, 1900223 (2019).
  - [36] Marzuola, J. L., Rechtsman, M., Osting, B. & Bandres, M. Bulk soliton dynamics in bosonic topological insulators. Preprint at <https://arxiv.org/abs/1904.10312> (2019).
  - [37] Mukherjee, S. & Rechtsman, M. C. Observation of Floquet solitons in a topological bandgap. *Science* 368, 856-859 (2020).
  - [38] Li, R. et al. Topological bulk solitons in a nonlinear photonic Chern insulator. *Commun. Phys.* 5, 275 (2022).
  - [39] Kartashov, Y. V., Malomed, B. A. & Torner, L. Solitons in nonlinear lattices. *Rev. Mod. Phys.* 83, 247-305 (2011).
  - [40] Lederer, F. et al. Discrete solitons in optics. *Physics Reports* 463, 1-126 (2008).
  - [41] Su, W. P., Schrieffer, J. R. & Heeger, A. J. Solitons in Polyacetylene. *Phys. Rev. Lett.* 42, 1698-1701 (1979).
  - [42] Hadad, Y., Soric, J. C., Khanikaev, A. B. & Alù, A. Self-induced topological protection in nonlinear circuit arrays. *Nat. Electron.* 1, 178-182 (2018).
  - [43] Wang, Y., Lang, L.-J., Lee, C. H., Zhang, B. & Chong, Y. D. Topologically enhanced harmonic generation in a nonlinear transmission line metamaterial. *Nat. Commun.* 10, 1102 (2019).
  - [44] Zangeneh-Nejad, F. & Fleury, R. Nonlinear Second-Order Topological Insulators. *Phys. Rev. Lett.* 123, 053902 (2019).
  - [45] Kotwal, T. et al. Active topoelectrical circuits. *Proc. Natl. Acad. Sci. U.S.A.* 118, e2106411118 (2021).
  - [46] Hohmann, H. et al. Observation of cnoidal wave localization in nonlinear topoelectric circuits. *Phys. Rev. Research* 5, L012041 (2023).
  - [47] Delplace, P., Ullmo, D. & Montambaux, G. Zak phase and the existence of edge states in graphene. *Phys. Rev. B* 84, 195452 (2011).
  - [48] Poli, C., Bellec, M., Kuhl, U., Mortessagne, F. & Schemm, H. Selective enhancement of topologically induced interface states in a dielectric resonator chain. *Nat. Commun.* 6, 6710 (2015).
  - [49] Kitagawa, T. et al. Observation of topologically protected bound states in photonic quantum walks. *Nat. Commun.* 3, 882 (2012).
  - [50] Zhang, W. et al. Observation of Bloch oscillations dominated by effective anyonic particle statistics. *Nat. Commun.* 13, 2392 (2022).